Numerical simulation of the performance characteristics, instability, and effects of band gap grading in cadmium telluride based photovoltaic devices

by

Michael David Petersen

A thesis submitted to the graduate faculty

in partial fulfillment of the requirements for the degree of

MASTER OF SCIENCE

Major: Electrical Engineering

Major Professor: Vikram Dalal

Iowa State University

Ames, Iowa

2001

Graduate College
Iowa State University

This is to certify that the Master's thesis of

Michael David Petersen

has met the thesis requirements of Iowa State University

Major Professor

For the Major Program

For the Graduate College

Table of Contents

ABSTRACT v
1 – INTRODUCTION 1
1.1 – History 1
1.2 – Numerical Models 2
1.3 – Organization 3
2 – PHOTOVOLTAIC DEVICES 4
2.1 – Solar Spectrum 4
2.2 – Materials 5
2.3 – Characterization 6
2.4 – Optimization 8
3 – AMPS-1D SIMULATOR 12
3.1 – Software Description 12
3.2 – Methods 13
4 – SIMULATIONS 15
4.1 – Front Interface Grading 15
4.1.1 – Absorber Layer With 1.7 eV Band Gap 15
4.1.2 – Absorber Layer With 1.5eV Band Gap 20
4.1.3 – Effects Of Discrete Grading 25
4.2 – Schottky Barrier Back Contact 27
4.2.1 – Effects on the IV curve 27
4.2.2 – Effects of Grading at the Back Interface 32
4.2.3 – Comparisons to Experimental Data 35
5 – CONCLUSION 38
APPENDIX A. SAMPLE AMPS CASE 40
APPENDIX B. DEGRADED IV CURVES 43
REFERENCES 44

ACKNOWLEDGEMENTS

I would like to thank my major professor, Vikram Dalal, for his time and support while pursuing my research and for convincing me to join the graduate program in the first place. His guidance was invaluable in completing this research. I would also like to thank Gary Tuttle and David Lynch for serving on my program of study committee. Another thanks goes to my fellow graduate students Roger Keen, Adam Sanford, and Paul Seberger whose moral support and sense of humor was invaluable.

Finally, and most importantly, I would like to thank my wife, Heather, for her patience, love, and support. Her encouragement and willingness to help support us financially made this work possible and enjoyable.

JS-T 2189

ABSTRACT

Using computer simulations, the performance of several CdTe based photovoltaic structures has been studied. The advantages and disadvantages of band gap grading, through the use of (Zn,Cd)Te, have also been investigated in these structures. Grading at the front interface between a CdS window layer and a CdTe absorber layer, can arise due to interdiffusion between the materials during growth or due to the intentional variation of the material composition. This grading has been shown to improve certain performance metrics, such as the open-circuit voltage, while degrading others, such as the fill factor, depending on the amount and distance of the grading.

The presence of a Schottky barrier as the back contact has also been shown to degrade the photovoltaic performance of the device, resulting in a characteristic IV curve. However, with the appropriate band gap grading at the back interface, it has been shown that the performance can be enhanced through more efficient carrier collection. These results were then correlated with experimental observations of the performance degradation in devices subjected to light and heat stress.

1 – INTRODUCTION

With the world's ever increasing energy demands, new and renewable energy sources are needed to sustain these energy needs. One renewable energy source available everywhere on earth is the sun's energy. Methods for harnessing this energy can take many forms from thermal to electrical conversion. Electrical methods using semiconductors convert the incident photon flux into a current while simultaneously producing a photovoltage, hence supplying power. The science and engineering behind these photovoltaics is continually evolving and improving as new materials, manufacturing methods, and device designs are discovered.

1.1 – History

As far back as 1839, scientists have known about the photovoltage phenomenon, discovered by Becquerel, where light impinging upon an electrode in an electrolytic solution would create a voltage [1]. In the 1870s, a similar effect was discovered in selenium and subsequent work led to the development of an approximately 1% efficient selenium photovoltaic cell used in photographic exposure meters. In the 1950s, work on silicon based photovoltaics increased rapidly with reports of a 6% efficient cell in 1954. Efficiencies as high as 14% had been reached by 1958. In addition to silicon, other material systems based on various sulfides, III-V compounds such as gallium arsenide, and II-VI compounds were also being studied. Through the next several decades, performance steadily improved and even more new material systems were discovered. Novel approaches for the physical design of the cell, such as the manipulation of the material properties and the stacking of several cells in tandem were also developed. By 2000, a 32.3% efficient, triple-junction cell had been reported [2].

In addition to improving the performance of the best cells, amorphous and polycrystalline materials have also being extensively studied. These materials do not provide the best photovoltaic efficiency when compared to crystalline materials, but they do allow very low-cost manufacturing methods to be used. Cost, an important consideration for any technology, is very important in most practical, terrestrial photovoltaic applications. While some applications, such as in space, are more concerned with efficiency and weight, low-cost

materials and manufacturing methods are very important in terrestrial applications where they must compete with traditional energy sources such as coal. The important parameter for terrestrial energy systems is the price per unit energy. If the cost of photovoltaic systems can be made low enough through the use of inexpensive materials, this ratio can be competitive with other forms of non-renewable energy.

1.2 – Numerical Models

In the development of photovoltaic devices, experimental methods have been used extensively to investigate different material and processing systems. While these methods are useful and necessary to prove theoretical assumptions, they make it difficult to control one variable without affecting many others. This is where numerical models can play a role. With a numerical model, individual parameters, such as the band gap, may be varied without necessarily affecting other parameters. This allows the investigator to examine the effects related directly to changes in one parameter. Also, the numerical model permits a variable to be changed over a wide range, possibly greater than can be achieved in a laboratory setting. Again, this provides insight into the effects of that one variable, even if these parameters are unrealistic or impractical.

Another advantage of numerical models is the ability to create an exact historical record of the experiments, showing exactly what changed between each case. Should an unexpected result be found, it is easy to reexamine the input parameters and deduce the causes of the result based on the changed parameters. Even with extensive record keeping and precision measurements, this might not be possible with traditional experimental methods since materials can change over time.

Despite the advantages of the numerical models, there are disadvantages. The main drawback is the inability to exactly model the semiconductor device. The numerical model is exactly that – a model. Therefore, any results obtained from numerical simulations must be considered within the constraints of that model. To apply the simulation results to actual devices, the correlation between the model and the real devices must be determined. In many cases, looking at the relative changes shown by the model may be more useful and universally applicable than looking at the absolute values obtained.

1.3 – Organization

The work described here examines the effects of several different optimizations that can be applied to photovoltaic devices, specifically cadmium telluride based devices. In some cases, these optimizations may be intentional and in others they may be due to the manufacturing process. In either case, the improvements and degradations in the properties of the photovoltaic device are studied through the use of numerical simulations. The mechanisms for these changes are also examined.

The simulations break down into two parts. The first is concerned with the interface between the window and absorber layers of the device. The introduction of band gap grading at this interface is studied. The second set examines the effects of a Schottky barrier as the back contact to the device. Again, the effects of band gap grading are also examined as a possible mechanism for improving the photovoltaic performance.

2 – PHOTOVOLTAIC DEVICES

2.1 – Solar Spectrum

Essential to the operation of photovoltaic devices is the light source. In most cases, this source is the sun. Therefore, the design of any practical photovoltaic device must be optimized for the particular solar radiation seen at the final application, be it in space or on earth. Since the radiation from the sun varies from one location to another, and from one time to another based on environmental conditions, several standards have been developed to provide a common method for comparison.

The sun itself can be closely modeled as a 6050°K blackbody radiator [1]. Deviations from the models can be attributed to the effects of the solar atmosphere and the variation in temperature across the sun's disk. At earth's mean distance from the sun, the solar energy is approximately 1353 kW/m^2 and is relatively constant. This radiation spectrum is designated as AM0. On the earth's surface, however, the solar radiation is more complex. Not only does the radiation vary depending on the latitude due to changes in the apparent atmospheric thickness, the absorption, scattering, and refraction in the atmosphere create peaks at characteristic wavelengths. The radiation on the earth's surface is designed AMx, where $x = \sec z$, and z is the angle from vertical. The average radiation is usually somewhere between AM1 and AM2, with the AM1.5 spectrum commonly used as a standard (Figure 1).

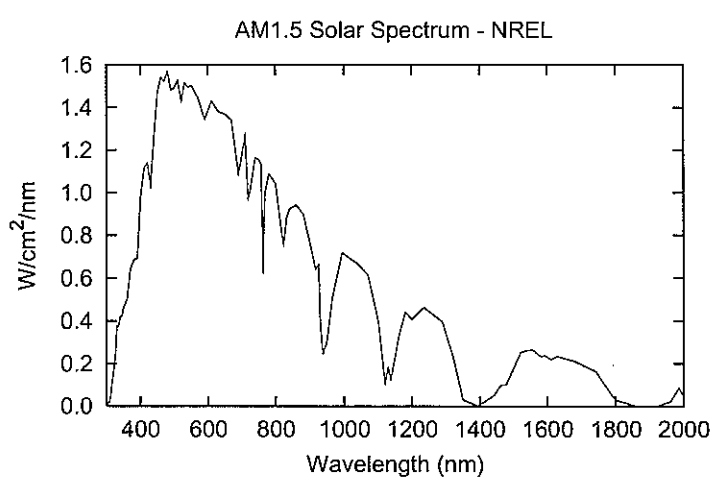

Figure 1: Standard AM1.5 spectrum (NREL)

Since the solar radiation is not constant with wavelength, and absorption in semiconductor materials varies with wavelength, a relationship between the two exists. As the band gap of the absorbing material decreases, the number of photons absorbed increases since more photons strike the material with an energy greater than the band gap. However, since the maximum voltage produced by a semiconductor junction is ultimately limited by the band gap, the small band gap materials consequently have low maximum voltages. On the other hand, large band gap materials can produce larger voltages, but fewer photons have enough energy to be absorbed by the material. In both cases, the limiting result is a reduction in the output power. However, at some intermediate band gap, the output power can be maximized, even though neither the voltage nor the current are at maximum. This optimal band gap has been calculated to occur around 1.5 eV for single junction devices.

2.2 – Materials

One of the most common photovoltaic materials is silicon. Being heavily used by the semiconductor industry for most semiconductor applications, silicon has many advantages, including the availability of high-purity materials, abundance of processing equipment, and significant processing knowledge. Unfortunately, as a photovoltaic material, crystalline silicon has some problems. The main drawbacks are its non-ideal band gap of 1.12 eV and its indirect optical absorption characteristics. Amorphous silicon can solve some of the problems with optical absorption and decrease cost, but the amorphous properties present new problems. Gallium arsenide (GaAs), another common photovoltaic material for high efficiency cells, does possess a near ideal band gap of 1.42 eV. Unfortunately, GaAs processing is quite expensive.

Cadmium telluride (CdTe) is receiving much interest lately as a photovoltaic material, especially for low-cost, terrestrial systems. With its near-ideal band gap voltage of 1.5 eV and the ability to form polycrystalline films, CdTe has long been recognized as a potential high-efficiency material for low-cost photovoltaic devices. Due to the material's large optical absorption coefficient, however, shallow junctions must be used to efficiently convert and collect the light energy. Without a shallow junction, most of the light would be absorbed in the bulk of the material, away from the junction's electric field, resulting in few of the carriers being collected. Unfortunately, forming a thin homojunction in CdTe with sufficient

conductivity is difficult [3]. Also, the high surface recombination velocity of CdTe presents problems with the homojunction design [4]. Therefore, a heterojunction configuration is usually used with the window layer having a larger band gap than the CdTe. This allows most of the light to be absorbed in the CdTe absorber layer and, with the assistance of the junction's built-in electric field, provides a more efficient collection of the carriers. Also, the heterojunction helps reduce surface recombination by preventing carriers from diffusing to the surface.

The window material best suited for use with CdTe has been found to be cadmium sulfide (CdS). With a band gap of 2.42 eV, CdS transmits most of the light within the visible spectrum. Also, as a thin film (<100 nm), CdS transmits significant portions of light with wavelengths below 500 nm which would otherwise be absorbed [5]. Since CdS can be easily doped highly n-type, a p-type CdTe absorber layer is usually used. Figure 2 shows a typical band diagram of the device.

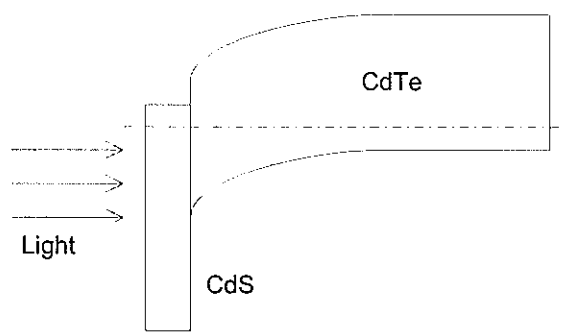

Figure 2: Typical CdS/CdTe device band diagram

2.3 – Characterization

Four main parameters characterize the performance of a photovoltaic device: short-circuit current (J_{SC}), open-circuit voltage (V_{OC}), fill factor, and efficiency. Short-circuit current is measured when the two terminals of the device are connected together through an ideally zero-resistance connection. Under thermal equilibrium conditions, no current would flow since the built-in voltage forces the diffusion and drift currents to exactly cancel. But, when light strikes the devices, thermal equilibrium no longer applies since the light generates excess carriers. These light generated carriers are swept out of the device by the internal electric field, increasing the drift current while the diffusion current remains the same,

resulting in a net flow of electrons from the p-type to the n-type side and holes from the n-type to the p-type side. This current is measured as the short-circuit current. While current flows under these conditions, no power is produced since no voltage exists between the device terminals.

The open-circuit voltage describes the performance of the illuminated cell with no electrical connections. In this case, the diffusion and drift currents must again equal as under thermal equilibrium conditions since there is no external path for the current. But, the light generated current must also be included. Since the light generated current contributes to the drift component, the built-in potential of the junction must decrease so as to bring the diffusion current into equilibrium with the drift current. In this process, the quasi-Fermi levels separate and a voltage is produced at the terminals of the device. However, no power is produced since no current flows.

Under conditions between short-circuit and open-circuit, the IV curve follows the same exponential shape as a normal PN diode, but shifted by the short-circuit current. Since parts of this curve fall within quadrant four, as shown in Figure 3, power is produced with a maximum power point occurring along the curve. The ratio of the maximum power divided by $J_{SC} \times V_{OC}$ is the fill factor and is a measure of the solar cell quality. Higher fill factors result in greater power at the maximum power point relative to the ideal rectangle bounded by J_{SC} and V_{OC}.

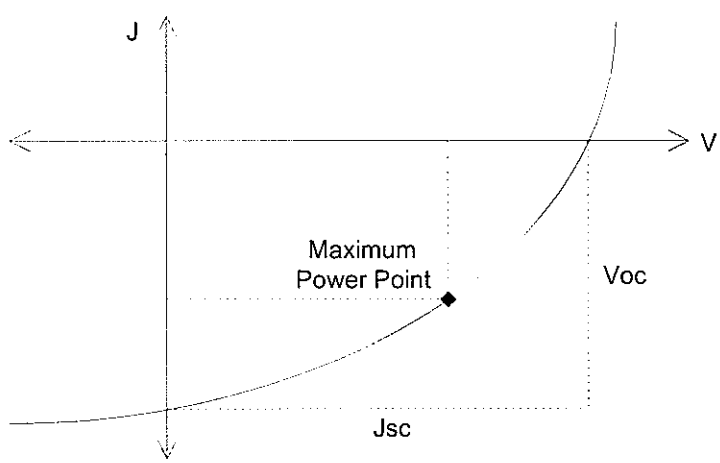

Figure 3: Typical IV curve

The fourth factor, efficiency, describes the ability for the photovoltaic device to convert the incident photon energy into electrical energy, relative to the total incident light energy. It can be expressed in terms of the power or collection efficiency. As a power, the efficiency of a photovoltaic device is the ratio of the power produced at the maximum power point of the incident light power. The quantum efficiency, on the other hand, is a measure of a photovoltaic device's ability to absorb photons and collect the resulting carriers, measured at a specific wavelength of light. The ratio of the incoming photon flux to the current is plotted against the wavelength, producing a spectral response (or quantum efficiency) curve for the device.

2.4 – Optimization

The use of heterojunction device configurations offers several advantages over the homojunction design. The heterojunction also introduces some practical considerations which, if unchecked, could significantly degrade the device performance. One such problem can arise when the band offsets produce a notch in either the conduction or valence band (Figure 4). These notches impeded the flow of electrons or holes, which may or may not be significant depending on the device configuration.

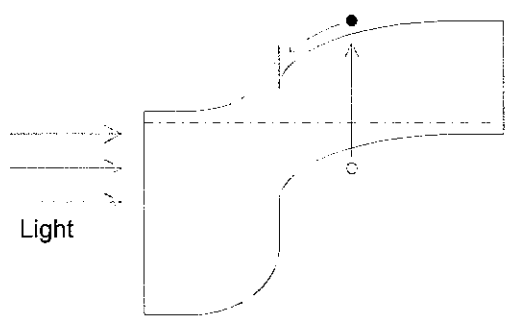

Figure 4: Trapping of electrons by conduction band notch

Another problem with heterojunctions is the lattice constant mismatch and thermal expansion mismatch between materials [1]. Unless the lattice constants or thermal expansion coefficients of the two materials in the heterojunction are perfectly matched, strain will be introduced in the crystal lattice during growth or temperature changes. Thermal expansion coefficient mismatches cause changes in the material properties, possibly affecting the device

performance at elevated temperatures. Lattice constant mismatches will result in some atoms not being bonded in the normal crystal pattern (Figure 5) or, if the strain is great enough and the material thick enough, the fracturing of the material. These unsatisfied bonds in the crystal lattice introduce defects which are very effective at trapping electrons and holes, resulting in a reduction in the carrier lifetime and diffusion lengths. Ultimately, these defects degrade the photovoltaic device efficiency. In thin-film materials, the effects of lattice constant mismatch may be minimized if the materials are kept thin, though this may not always be possible due to other optimization concerns.

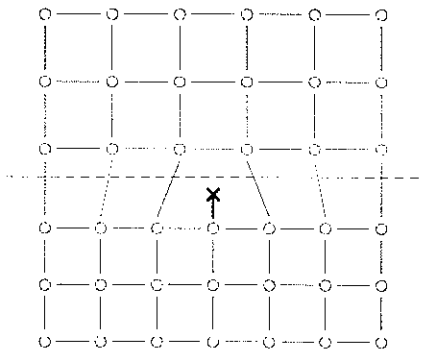

Figure 5: Defect caused by lattice constant mismatch

Despite these drawbacks of heterojunction devices, there are many advantages, some of which allow the reduction or elimination of the problems above. One advantage of heterojunctions is the ability to reduce surface recombination. By placing a wide band gap material with the appropriate band offsets at the surface of a device, the generated minority carriers can be prevented from reaching the surface and recombining. Additionally, with many heterojunction materials, the change from one material to another can be made gradually by careful selection and control of growth conditions. This gradual change in material results in the grading of various material parameters, including the band gap, electron affinity, and lattice constant. The exact changes and degree of variation which are possible are determined by the materials used [1, 6].

By gradually changing the lattice constant, the strain introduced by lattice mismatch can be reduced, hence reducing or, at the least, spreading the defect density over the graded region. Also, the ability to grade the conduction and valence bands introduces additional

effective electric fields for electrons and holes. The fields can be found by Equation 1 for electrons and Equation 2 for holes [7].

Equation 1: $\mathscr{E}_{neff} = \frac{\partial E_C}{\partial x} = \frac{\partial \chi}{\partial x} + kT\frac{\partial}{\partial x}(\ln N_C)$

Equation 2: $\mathscr{E}_{peff} = \frac{\partial E_V}{\partial x} = \frac{\partial}{\partial x}(\chi + E_G) - kT\frac{\partial}{\partial x}(\ln N_V)$

These electric fields force the carriers away from the graded region, and therefore, away from the region of high defect density, reducing recombination. This is shown schematically in Figure 6. Similarly, electric fields can be used at the surface to drive carriers away and reduce the surface recombination effects.

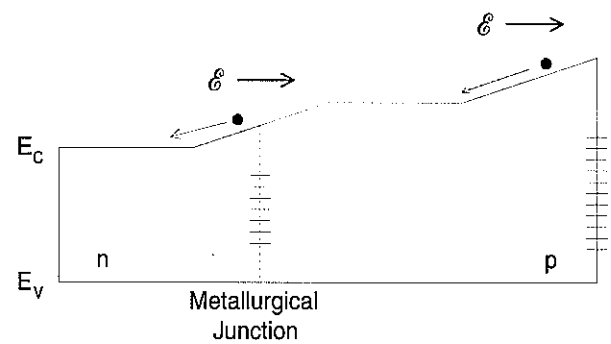

Figure 6: Band grading used to force carriers away from defects

An additional improvement may also be obtained with band grading through the increase in diffusion length due to the electric field. The effective diffusion length in the presence of an electric field is described in [1] and can be approximated by Equation 3, where $\mathscr{E}$ is the electric field and L_{n0} is the diffusion length without the electric field.

Equation 3: $L_{eff} \cong L_{n0}\left(\frac{\mathscr{E}\, q\, L_{n0}}{kT}\right)$

As the electric field increases, the diffusion length increases, increasing the probability that the generated carriers will be collected without recombining. This should result in an improvement in the quantum efficiency.

In the CdTe material system, band grading can be accomplished through the use of (Zn,Cd)Te. Since CdTe and ZnTe have nearly zero offset in the valence band [8], the greatest band variation can be obtained in the conduction band due to the different band gaps of 1.50 eV and 2.25 eV, respectively. Also, CdTe and ZnTe form a continuous series of solid solutions, allowing a wide variation in the material properties. The band gap variation for a $Cd_{1-x}Zn_xTe$ compound at 300K as a function of composition, x, is given by Equation 4 [9].

Equation 4: $E_G(eV) = (1.510 \pm 0.005) + (0.606 \pm 0.010)x + (0.139 \pm 0.010)x^2$

In addition to intentional variation of the band gap through the use of (Zn,Cd)Te, the band gap can also vary due to interdiffusion between the materials used to fabricate the device. For example, the CdS/CdTe interface has been the subject of much research. The interdiffusion between these materials can lead to a smoothing of the conduction band offset resulting in a grading of the band gap. Since the lattice mismatch between CdS and CdTe is 9.7% and each material crystallizes into different structures, significant problems can occur at the interface, presumably resulting in low efficiencies [10]. Despite these differences, though, high efficiency devices have been fabricated using a $CdCl_2$ treatment and annealing. The interdiffusion during these steps likely improves the interface by smoothing the transition and reducing the defect density [11]. However, excessive interdiffusion has also been reported to degrade the spectral response in the blue and green wavelengths.

3 – AMPS-1D SIMULATOR

3.1 – Software Description

The simulation engine for this research is the AMPS-1D program, written by Professor Stephen Fonash and his students at The Pennsylvania State University. This program simulates a wide variety of one-dimensional microelectronic and photonic devices, the structure of which are mostly controlled by the user. The Microsoft Windows version of the software (Beta v.1) was used in this research. This version provides a graphical user interface for inputting device parameters and layer characteristics.

The following description of AMPS is a summary of the detailed description contained in the manual provided with the software. The principal equations solved by AMPS are Poisson's equation (Equation 5), the continuity equation for electrons (Equation 6), and the continuity equation for holes (Equation 7).

Equation 5: $$\frac{\mathrm{d}}{\mathrm{d}x}\left(-\varepsilon(x)\frac{\mathrm{d}\Psi'}{\mathrm{d}x}\right) = q\cdot\left[p(x) - n(x) + N_D^{+}(x) - N_A^{-}(x) + p_t(x) - n_t(x)\right]$$

Equation 6: $$\frac{1}{q}\left(\frac{\mathrm{d}J_n}{\mathrm{d}x}\right) = -G_{op}(x) + R(x)$$

Equation 7: $$\frac{1}{q}\left(\frac{\mathrm{d}J_p}{\mathrm{d}x}\right) = G_{op}(x) - R(x)$$

In Poisson's equation, Ψ' is the electrostatic potential, n and p are the free electron and hole concentrations, n_t and p_t are the trapped electron and hole concentrations, and N_D^+ and N_A^- are the ionized donor and acceptor doping concentrations, all functions of position. In the continuity equations, J_n and J_p are the electron and hole current densities and R and G_{op} are the recombination and optical generation rates, respectively.

Each of these equations has two associated boundary conditions which are used to solve for a set of state variables at each point in the device. These state variables are the electrostatic potential, the electron quasi-Fermi level, and the hole quasi-Fermi level. From

these three state variables, all other quantities can be computed. The method of finite differences and the Newton-Raphson technique are used to iteratively solve these equations for each point in the device. Once these solutions are found, the remaining quantities are determined.

A range of input parameters is available to the user, describing the electrical and physical properties of each layer in the device. Since the parameters are input as physical quantities (permitivity, band gap, electron affinity, doping, etc.), a wide variety of materials may be simulated, even materials without direct equivalents in nature. This is useful in understanding the effects of a specific variable upon device performance, but may hinder the application of the simulation results to real devices. In addition to describing the characteristics of each layer, the illumination, biasing, and contacting to the device may also be specified. One limitation, though, is the inability to model tunneling at the contact interfaces. However, a workaround for this problem, when the model calls for a tunnel barrier, is to match the metal work function with the semiconductor Fermi level and adjust the surface recombination velocity appropriately.

3.2 – Methods

For the simulations in this research, a basic case with the essential parameters and layers was developed. This case was then copied multiple times, and these copies modified to produce the parameter sweeps being investigated. These groups of cases with various parameter sweeps were then queued together and simulated by AMPS, generally taking several hours to complete. The resulting data were then analyzed in the AMPS graphing utility, exported as an ASCII table for analysis in a spreadsheet, or transcribed to a spreadsheet by hand via the Windows clipboard (copy & paste).

Table 1 lists the basic material parameters used for the simulations in this research. A more detailed listing of the parameters for a sample case, including the absorption coefficients, is listed in Appendix A. While these parameters were sometimes varied and not all of the following materials used, these are the fundamental parameters and materials used for constructing the basic simulation cases. Also, when a parameter was to be varied within a single case, multiple layers were created, each with this particular parameter slightly changed.

Table 1: Basic material parameters for simulations

Parameter	AMPS variable	CdS	CdTe	ZnTe	Units
Relative permitivity (ε_s)	EPS	9.0	9.4	9.0	
e^- mobility (μ_n)	MUN	350	500	1 [(a)]	$cm^2/V\cdot s$
h^+ mobility (μ_p)	MUP	50	60	1	$cm^2/V\cdot s$
Band gap (E_g)	EG	2.42	1.50	2.25 [(b)]	eV
Conduction band DOS (N_c)	NC	$1.8\cdot10^{19}$	$7.5\cdot10^{17}$	$7.5\cdot10^{17}$	cm^{-3}
Valence band DOS (N_v)	NV	$2.4\cdot10^{18}$	$1.8\cdot10^{18}$	$1.8\cdot10^{18}$	cm^{-3}
Electron affinity (χ)	CHI	4.50	4.28	3.50	eV
Acceptor doping	NA	—	$1\cdot10^{15}$	$1\cdot10^{18}$	cm^{-3}
Donor doping	ND	$1\cdot10^{18}$	—	—	cm^{-3}
<u>Gaussian Acceptor & Donor Defects</u>					
Density	NAG	—	$1\cdot10^{13}$	—	cm^{-3}
	NDG	$1\cdot10^{13}$	—	—	cm^{-3}
Energy	EACPG	—	0.76	—	eV
	EDONG	1.24	—	—	eV
Width	WDSAG	—	0.01	—	eV
	WDSDG	0.01	—	—	eV
Electron capture cross-section	GSIG/NA	—	$6.25\cdot10^{-11}$	—	cm^2
	GSIG/ND	$5\cdot10^{-10}$	—	—	cm^2
Hole capture cross-section	GSIG/PA	—	$6.25\cdot10^{-10}$	—	cm^2
	GSIG/NA	$5\cdot10^{-11}$	—	—	cm^2

[a] Reference [8]
[b] Reference [9]

4 – SIMULATIONS

4.1 – Front Interface Grading

In this set of simulations, a solar cell with a CdS window layer, (Zn,Cd)Te absorber layer, and a highly doped ZnTe back contact was investigated. The purpose of these simulations was to examine the effects of band gap grading in the (Zn,Cd)Te layer at the front interface, as shown schematically in Figure 7. This grading can arise from intentional variation of the Zn-to-Cd ratio or by interdiffusion between the CdS window layer and the CdTe absorber layer. The distance of the grading was varied from 3 nm to 1000 nm and was done with a total band gap change of 0.2 eV.

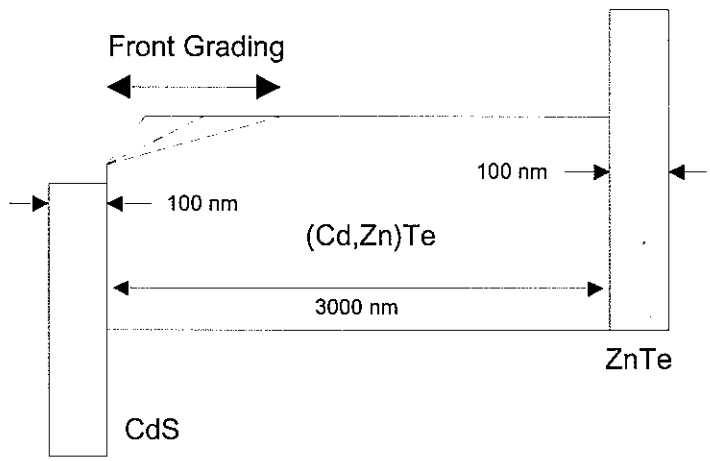

Figure 7: Schematic representation of band gap grading at the front interface

4.1.1 – Absorber Layer With 1.7 eV Band Gap

The IV curves provide a qualitative view of the changes due to band gap grading at the front. Some of the deficiencies in this model can also be observed in the following graphs. The curves in Figure 8 and Figure 9 are for a case where the band gap started at 1.5 eV at the front interface and was graded up to 1.7 eV from that amount. This represents intentional grading through the use of (Zn,Cd)Te in the bulk of the absorber layer. Figure 8 shows the case when the optical absorption coefficient is constant and Figure 9 shows the case when the absorption coefficient shifts in correspondence with the band gap.

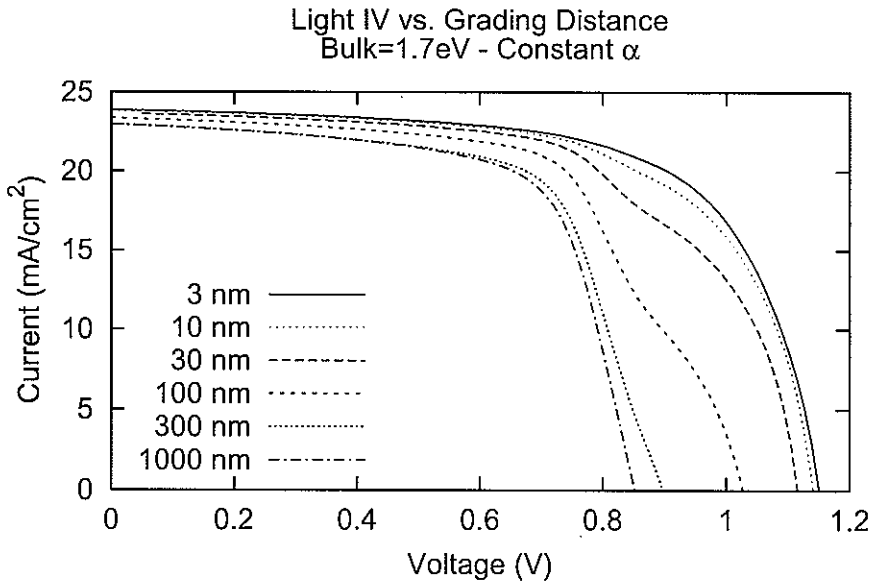

Figure 8: IV curves for grading at the front interface, 1.7 eV absorber band gap, Constant α

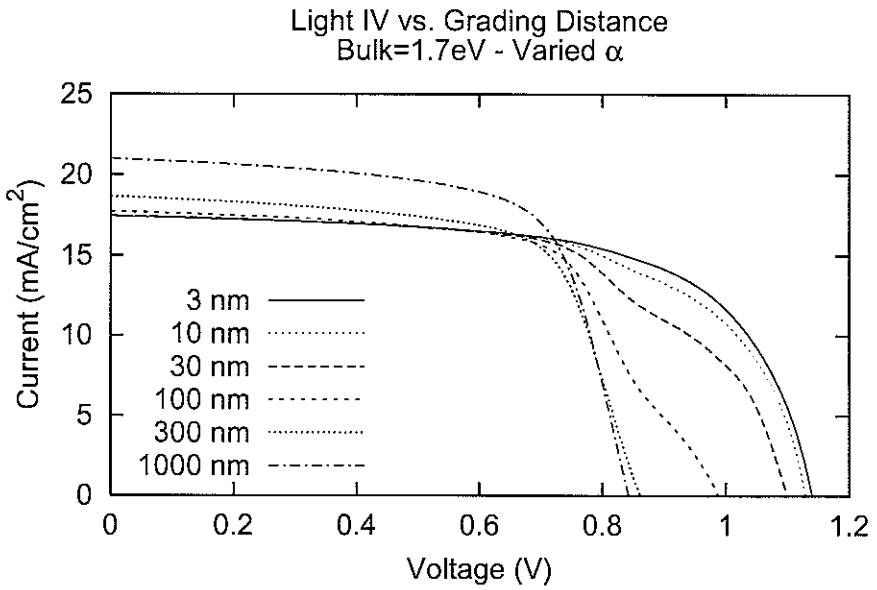

Figure 9: IV curves for grading at the front interface, 1.7 eV absorber band gap, Varied α

The trends in the short-circuit current differ between the two cases, due to the differences in the optical absorption coefficients. When the absorption coefficient is constant, the short-circuit current decreases as the grading distance increases. Since the optical absorption coefficient is constant, the generation rate remains constant, regardless of the band gap. But, as the grading distance increases and the effective conduction band electric field therefore decreases, the electron diffusion into the CdTe region, which opposes the short-circuit current, is increased. Therefore, since this diffusion of electrons increases and the generation of new carriers remains constant, the short-circuit current drops.

On the other hand, when the absorption coefficient varies with the band gap, the short-circuit current increases with increasing grading distance. While the opposing diffusion of electrons is still a factor as in the first case, the increased distance over which a small band gap is present is the dominant factor. This smaller band gap results in a larger generation rate over a greater distance near the front surface (Figure 10) which, in this model, is more important than the increases in diffusion due to the more gradual grading.

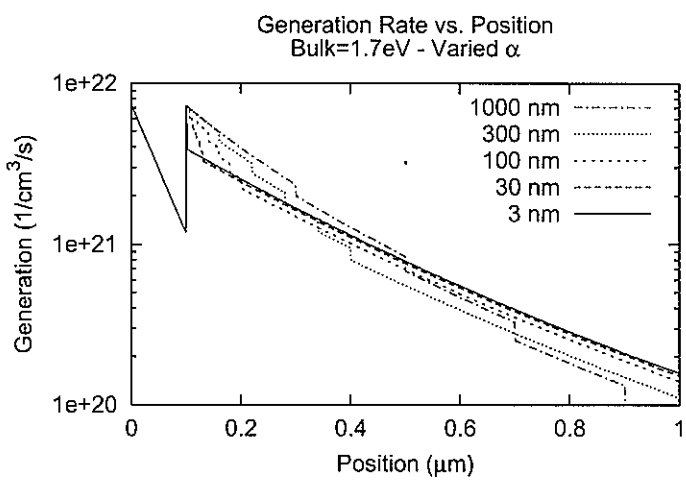

Figure 10: Generation rate for varying absorption coefficients

Since the results obtained for the short-circuit current vary greatly depending on the model parameters, the absorption coefficient in this case, this model is not adequate for predicting or analyzing these changes. However, between the two cases, the trends in open-

circuit voltage and fill factor are the same, and therefore, the effects of grading upon these parameters can be studied.

The variations in the open-circuit voltage due to grading are shown in Figure 11. The open-circuit voltage increases as the grading distance decreases. As the grading distance decreases, the device begins to approximate an ideal heterojunction with a greater conduction band offset, therefore providing a greater separation of carriers, hence allowing more separation between the quasi-Fermi levels (Figure 12). This greater separation contributes to a larger terminal voltage in open-circuit conditions.

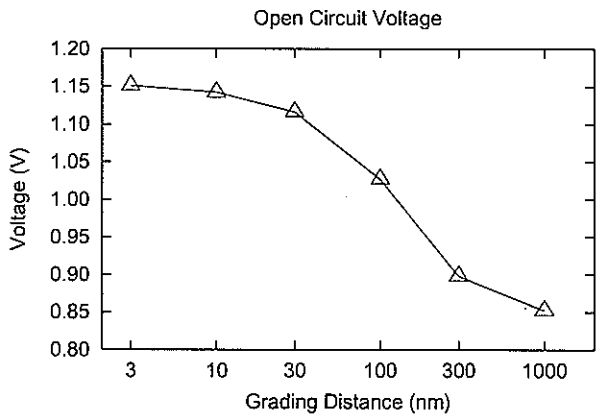

Figure 11: Open-circuit voltage variation due to band gap grading with 1.7 eV absorber band gap

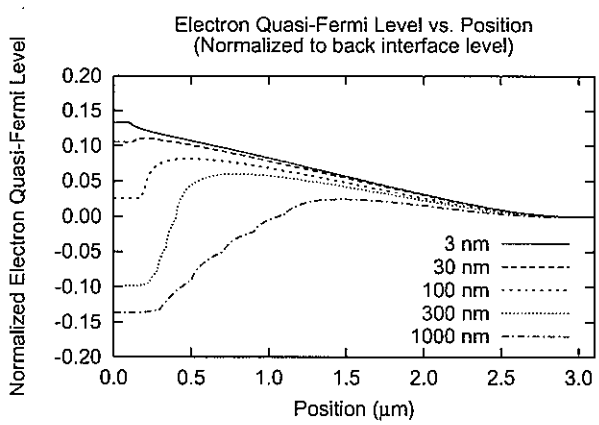

Figure 12: Normalized electron quasi-Fermi levels versus position

The fill factor also changes as the front interface band gap is graded as shown in Figure 13. As the grading goes from very short distances to longer distances, the fill factor degrades, then improves again. Referring back to Figure 8 and Figure 9, the reduction in fill factor corresponds to those grading distances which produce "kinking" in the IV curves. The fill factor is reduced since the maximum power point occurs at nearly the same voltage despite the greater increase in the open-circuit voltage (Figure 14). Hence, the maximum power point rectangle grows more slowly than the $I_{SC}xV_{OC}$ rectangle, reducing the fill factor.

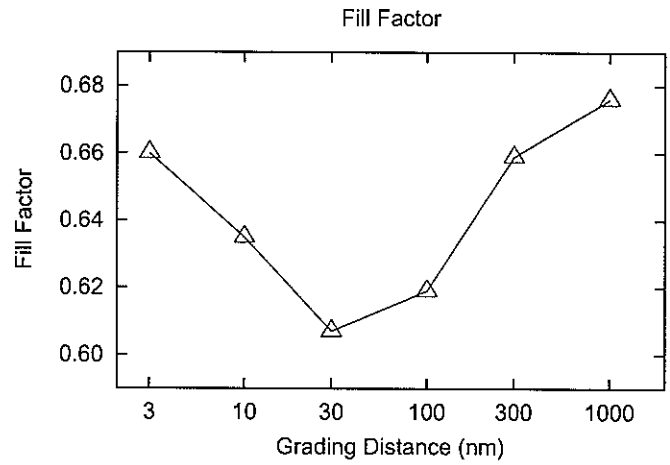

Figure 13: Fill factor variation due to band gap grading with 1.7eV absorber band gap

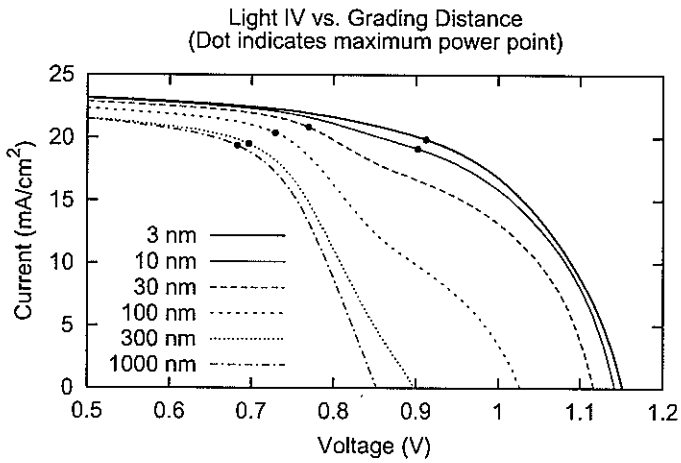

Figure 14: Variation in maximum power point for "kinked" IV curves

It can also be observed in Figure 14 that the kink occurs around a bias of 0.9 V. This corresponds to the junction's built-in voltage. At low biases, the IV curve changes as would be expected with a traditional PN junction. In a traditional PN junction, when the applied bias approaches the built-in potential, the drift and diffusion currents would be nearly equal, resulting in zero net current. However, with the graded band gap and conduction band offset, an effective conduction band electric field still exists at this bias and helps to continue sweeping carriers out of the device. The conduction band offset works in much the same way, keeping the opposing diffusion of electrons low and the net electron current flowing toward the front. Thus, the IV curve flattens as the bias is increased. At some point, the applied bias is great enough to counteract the grading induced electric field and band offset to such a degree that the diffusion and drift currents become equal and the net current then goes to zero. The voltage at which the net current goes to zero, however, is greater than if the grading was not present and assisting the collection of electrons.

4.1.2 – Absorber Layer With 1.5eV Band Gap

The IV curves in Figure 15 and Figure 16 are for the case when the band gap was graded from 1.3 eV to 1.5 eV, representing interdiffusion between the CdS window layer and the CdTe absorber layer. This eliminated the conduction band discontinuity normally assumed to be present at the interface. The "0 nm" case, however, represents the ideal CdS/CdTe interface. The difference between a constant absorption coefficient (Figure 15) and a varied absorption coefficient (Figure 16) is much less than before, only exhibiting an effect for a large grading distance and low biases due to the greater generation rate of the smaller band gap which penetrates deeper into the device.

The most notable feature of these curves, as compared to the previous set, is the lack of any kinking in the IV characteristics. This can be attributed to the lack of any conduction band offset combined with grading. In the previous set of simulations, the conduction band offset was present along with the grading induced electric field. In these simulations, however, the conduction band offset was not present. Another way of looking at this is to consider the conduction band offset as band gap grading over a very small distance (the limit as the distance goes to zero). In the previous set of simulations with a 1.7 eV absorber layer, two gradings were therefore present: the band offset and the more gradual band gap grading.

However, in this set of simulations, only one grading was present, and this grading happens to resemble the band offset as the distance goes to zero. Without the band offset always present, the transition from drift dominated net current to diffusion dominated net current is more gradual as the bias is changed, resulting in the normal IV curve shape.

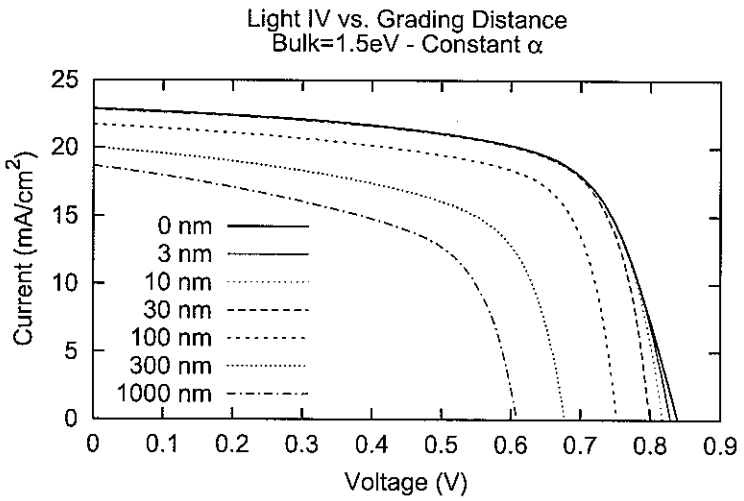

Figure 15: IV curves for grading at the front interface, 1.5 eV absorber band gap, Constant α

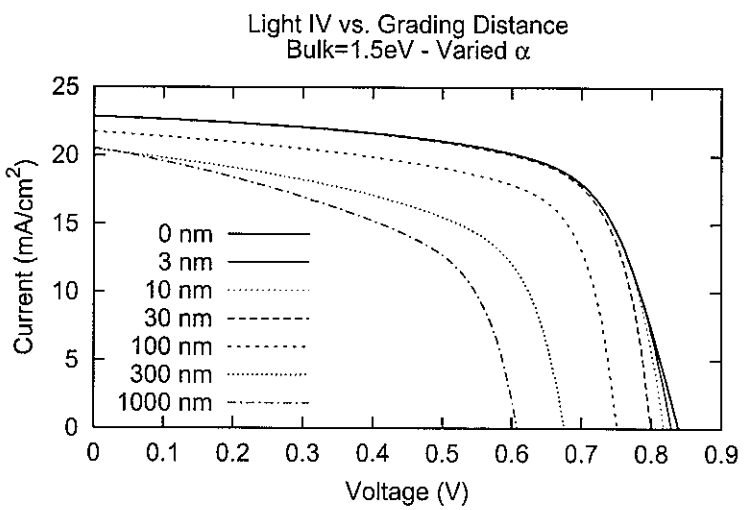

Figure 16: IV curves for grading at the front interface, 1.5 eV absorber band gap, Varied α

To verify that the band offset was the cause of the IV curve kinking, the first set of simulations with an absorber band gap of 1.7 eV were simulated again, this time with the CdS layer shifted up 0.2 eV to eliminate the band offset at the interface. The resulting IV curves are shown in Figure 17. This confirms that the kinking is mostly due to the presence of the band offset. However, as shown in Figure 8 and Figure 9, some band gap grading must also be present.

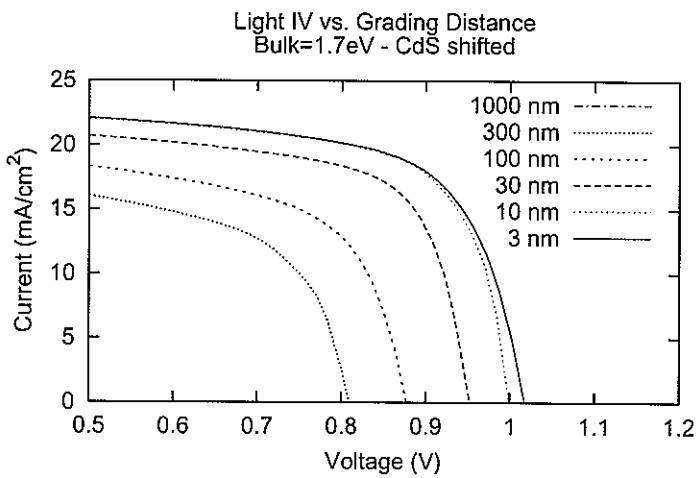

Figure 17: IV curves with a shifted CdS layer, 1.7 eV absorber band gap

Referring again to the case with a 1.5 eV absorber band gap (Figure 15 and Figure 16), the open-circuit voltage increases as the band gap is graded over shorter distances. However, the fill factor changes in a much different manner than in the 1.7 eV absorber case. As shown in Figure 18, the fill factor increases as the grading distance increases, mainly due to the reduction in the open-circuit voltage without a corresponding reduction in the low-bias current. However, at larger grading distances, the fill factor drops off as the short-circuit current decreases (Figure 19) along with the open-circuit voltage (Figure 20).

The decrease in the short-circuit current can be attributed to the presence of a small band gap over a larger region of the device which in turn results in greater band-to-band recombination (Figure 21). This increase in recombination reduces the current, though only at larger grading distances where it can affect a greater number of carriers.

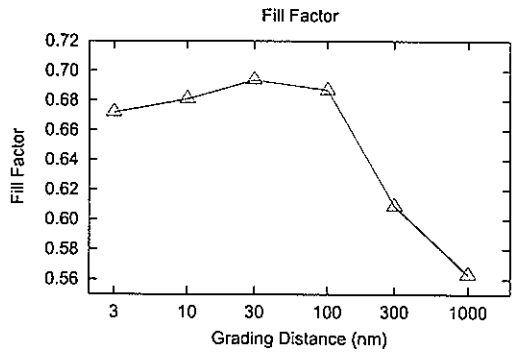

Figure 18: Fill factor variation due to band gap grading with 1.5 eV absorber band gap

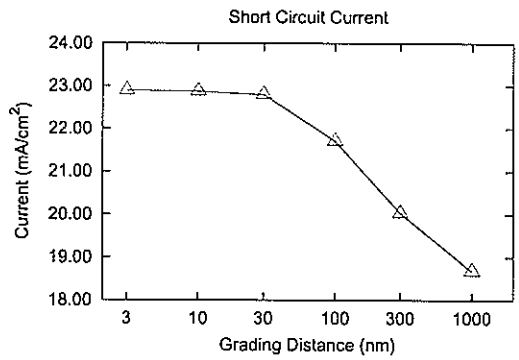

Figure 19: Short-circuit current variation due to band gap grading with 1.5 eV absorber band gap

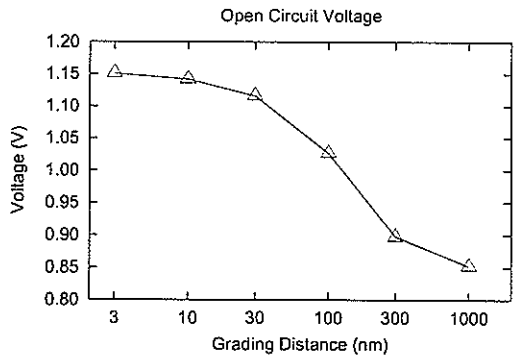

Figure 20: Open-circuit voltage variation due to band gap grading with 1.5 eV absorber band gap

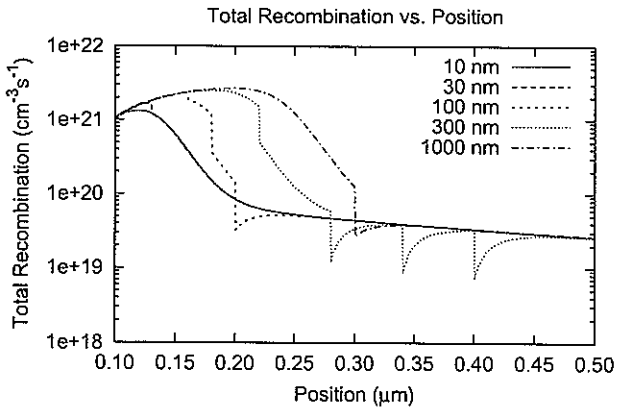

Figure 21: Carrier recombination at the front interface for various grading distances

The decrease in short-circuit current can also be explained by the reduction in spectral response at the short wavelengths (Figure 22). As reported in the literature, the short-wavelength spectral response in the simulations decreases with an increase in the grading distance. This agrees with the observations reported on devices with excessive interdiffusion at the interface.

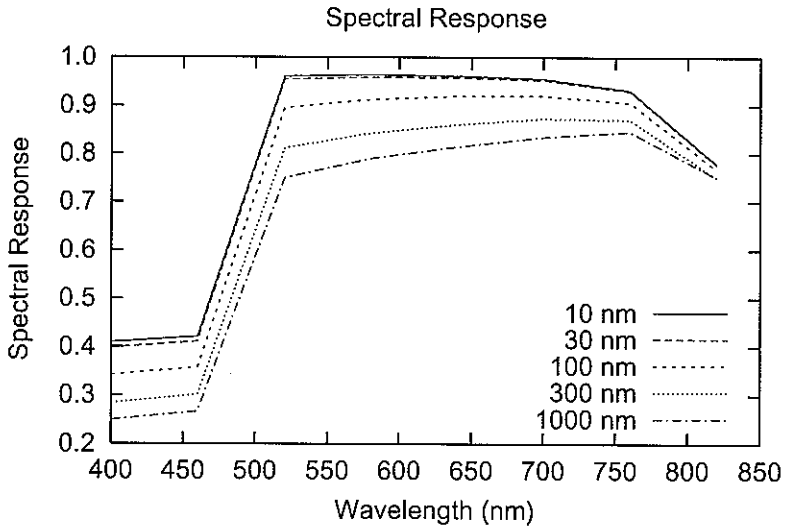

Figure 22: Spectral response for various grading distances

4.1.3 – Effects Of Discrete Grading

Finally, to help validate these results and see the effects of using discrete layers to simulate the band gap grading, a set of simulations was run for select cases above (grading distance of 100 nm). The number of layers in the graded region was increased and the layers were made thinner to better approximate a continuous grading. While a real device would likely be manufactured using discrete layers, theoretically creating a step-like grading, in most cases interdiffusion between the layers would likely spread the grading, making it more continuous. Therefore, the simulation's sensitivity to the step-like grading is important in determining the validity of the above results. Figure 23 shows the effects of using a different number of layers in the graded region.

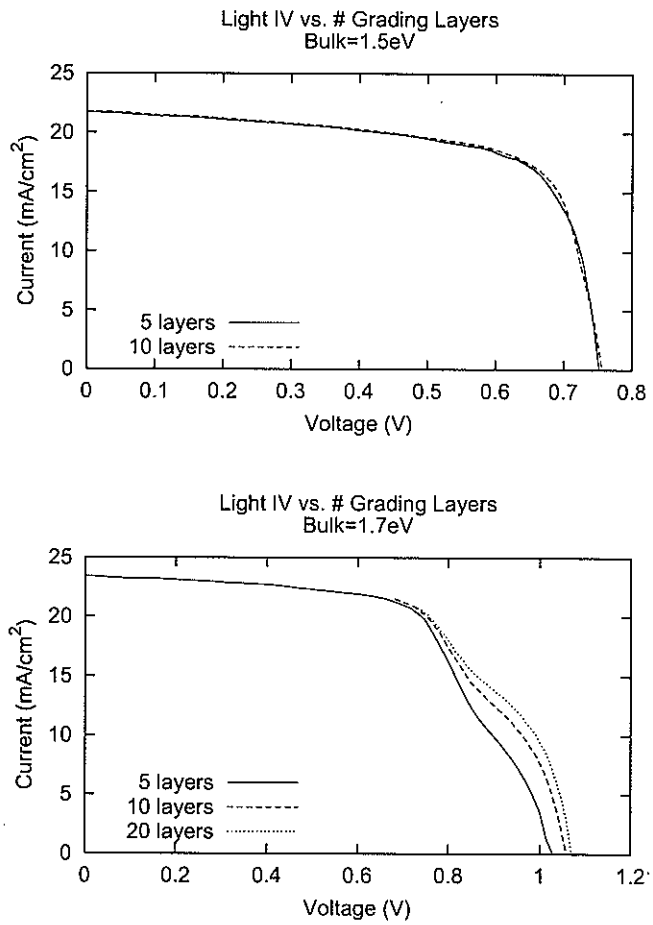

Figure 23: Effects of the number of layers in the graded region

For the 1.5 eV absorber layer, where no conduction band offset was present, the use of a different number of layers in the graded region had little effect upon the resulting IV curve. For the 1.7 eV absorber layer, however, where the conduction band offset was present, the effect of a different number of layers is more pronounced. As the graded region approaches a continuous grading (more and thinner layers), the open-circuit voltage increases and the kinking becomes more prominent. This can be attributed to the more constant electric field in the conduction band. Although the average field is the same, its distribution is different. With larger layers, the field is strong at the step edges, but weak between them. However, with thinner layers, the steps are smaller but more frequent, leading to a more continuous field throughout the graded region (Figure 24). This continuous field is more effective than the field with bigger, but fewer, steps. While the same effects are also present in the case with no conduction band offset, they are more important when the conduction band offset is present since the band offset itself is already quite effective in preventing electron diffusion from the CdS to CdTe. The larger layers, with their discontinuous field, reduce the forces opposing this diffusion and cause the net current to decrease for a particular applied bias, as shown in Figure 23.

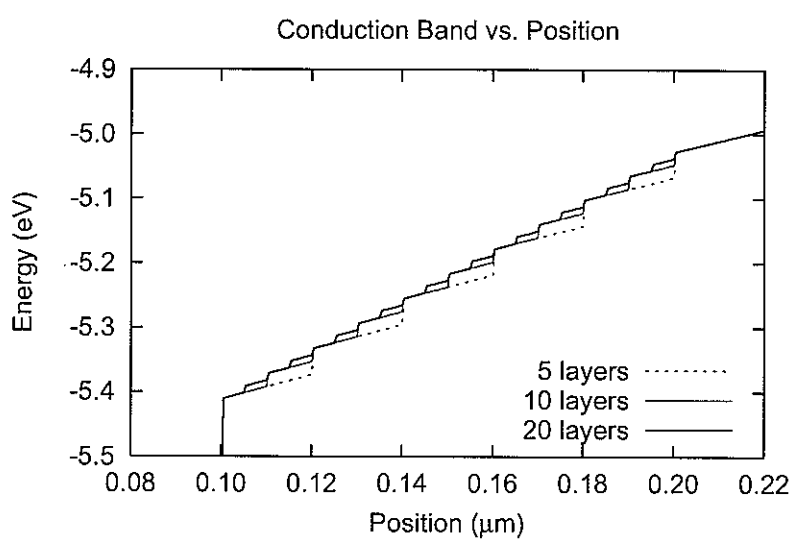

Figure 24: Conduction band edge in the graded region, 1.7eV absorber band gap

4.2 – Schottky Barrier Back Contact

In this set of simulations, a photovoltaic device with a CdS window layer, a CdTe absorber layer, and a Schottky barrier back contact was investigated (Figure 25). In some cases, a 500 nm region of lower doping was used near the back contact. The purpose of these simulations was to examine the effects of the Schottky barrier and the lightly doped region on the IV characteristics of the device and to investigate the physical cause of the changes. Barrier heights ranging from 0.0 eV to 1.0 eV were used along with doping levels from 10^{12} cm^{-3} to 10^{15} cm^{-3} in the back region. Finally, the use of band gap grading at the back interface in the presence of the Schottky barrier back contact and lightly doped region was studied as a possible method for improving the carrier collection efficiency.

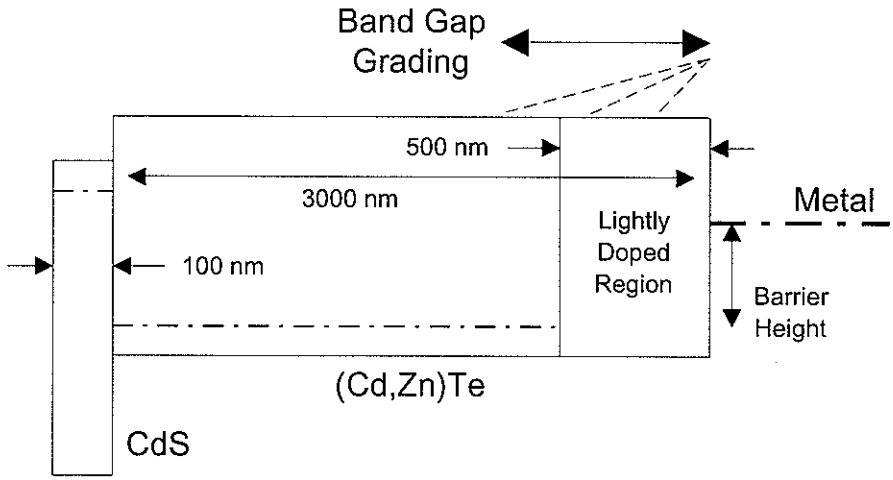

Figure 25: Schematic representation of the device with Schottky barrier back contact and lightly doped region

4.2.1 – Effects on the IV curve

The effects of various Schottky barrier heights on the IV characteristics of the devices with a constant doping of 10^{15} cm^{-3} are shown in Figure 26. For small barrier heights, the IV characteristics are close to the expected shape. However, as the barrier height increases, the curve flattens as the bias approaches the open-circuit voltage. The short-circuit current and open-circuit voltage also decrease as the barrier height increases.

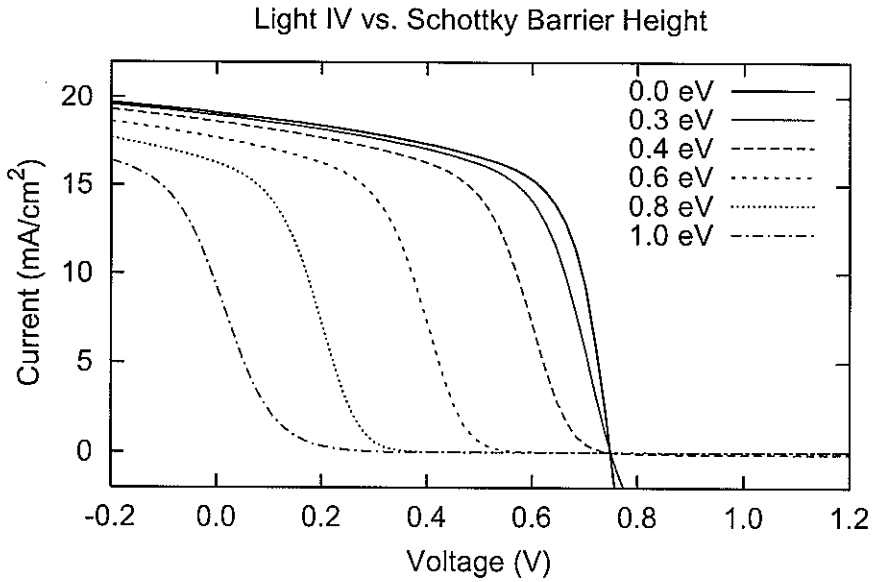

Figure 26: IV characteristics for various Schottky barrier heights

This flattening of the IV curve in the forward bias region can be attributed to the Schottky diode created at the back contact. This diode is in opposition to the flow of forward (non-power producing) current in the main photovoltaic device (Figure 27). As the bias increases, the current saturates at some small value which corresponds to the reverse current for the particular Schottky diode contact. During normal operation of the photovoltaic device, when it is producing power, the Schottky diode is forward biased and has a minimal effect on the IV curve shape in this region.

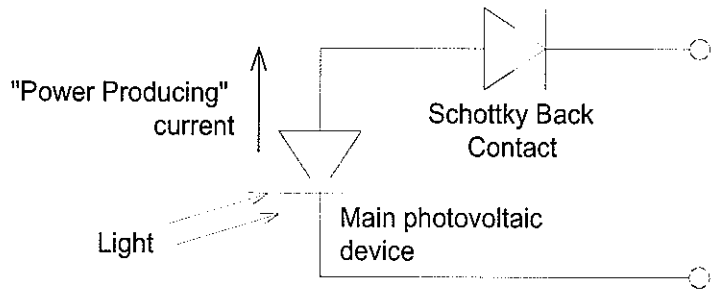

Figure 27: Circuit schematic for a device with a Schottky barrier back contact

The introduction of a lightly doped region at the back contact also affects the IV characteristics as shown in Figure 28, Figure 29, and Figure 30. The effects, however, only appear to be significant when the Schottky barrier has already degraded the performance. Therefore, barrier heights from 0.2 eV to 0.4 eV were examined. The flattening of the IV curve near the open-circuit voltage is still evident. However, as the doping is decreased, the flattening becomes more severe. All of these effects may be traced back to the detrimental band bending caused by the Schottky barrier (Figure 31). The introduction of a lightly graded region only worsens these effects by enhancing the built-in electric field in this region and therefore enhancing the flow of current in the direction opposite the direction needed to produce power.

Referring again to Figure 31, it can also be observed that the band bending at the back of the device due to the Schottky barrier introduces a field opposing the desired flow of electrons at the back contact. This field sweeps electrons toward the back contact and pushes holes away, exactly opposite of the direction needed for efficient carrier collection. Therefore, the introduction of a complementary electric field near the back could assist in collecting the minority carrier electrons. A band gap graded layer, using (Zn,Cd)Te could provide such a field in the conduction band.

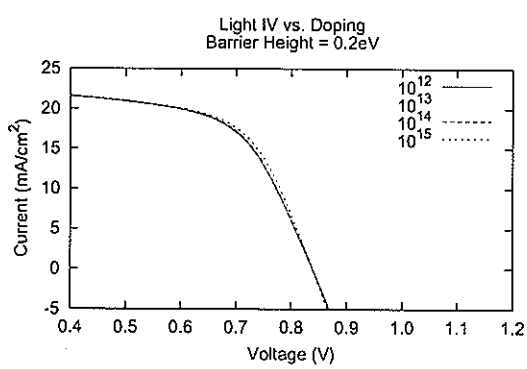

Figure 28: IV characteristics for various back-region doping densities, 0.2 eV barrier height

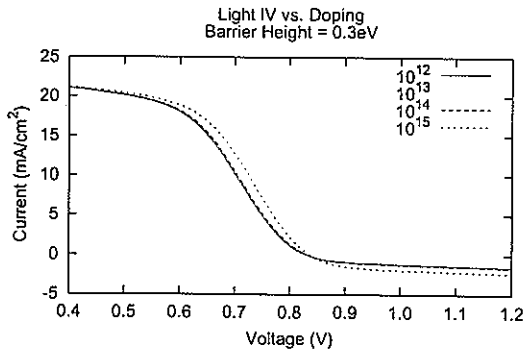

Figure 29: IV characteristics for various back-region doping densities, 0.3 eV barrier height

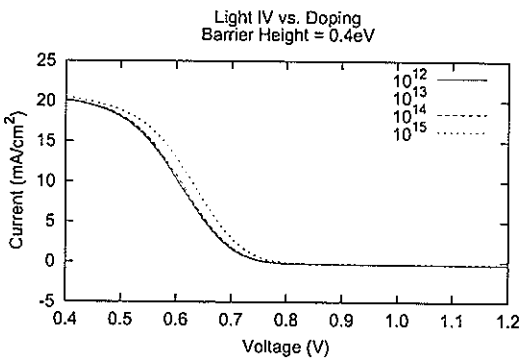

Figure 30: IV characteristics for various back-region doping densities, 0.4 eV barrier height

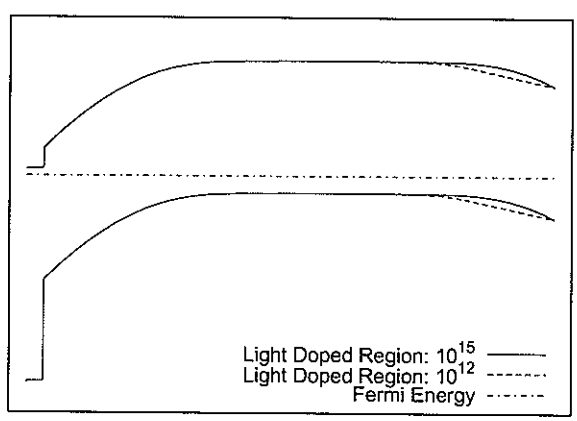

Figure 31: Band diagram for Schottky barrier back contact with various doping densities

Another parameter characterizing the degradation in performance due to the Schottky barrier is the ratio between the quantum efficiency at the maximum power point and the quantum efficiency under short-circuit conditions. Sharp IV curves (and large fill factors) are characterized by QE ratios near 1.0 since the current collection does not decrease much as the bias increases. However, the QE ratio will never be exactly 1.0 since some reduction in current collection will occur, even in the best devices. Small QE ratios, on the other hand, are indicative of small fill factors and a significant reduction in current collection under an applied bias. Figure 32 and Figure 33 show the simulated QE ratio as a function of wavelength for various back-region doping densities and barrier heights.

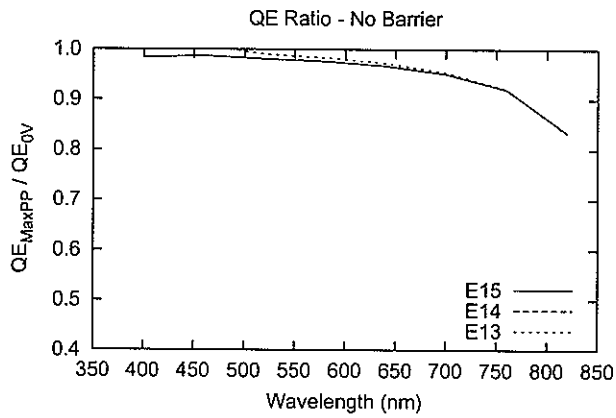

Figure 32: QE ratio for 0.0 eV barrier height

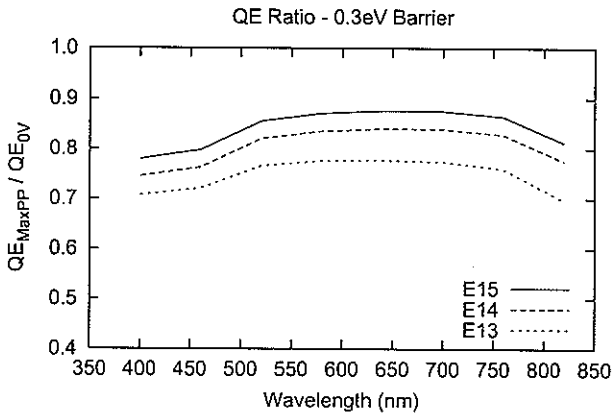

Figure 33: QE ratio for 0.3 eV barrier height

The reduction in the QE ratio seen in this data can be attributed to the combined effects of the Schottky barrier and reduced back-region doping density. When no Schottky barrier is present (Figure 32), the QE ratio decreases the same amount at the long wavelengths for all doping densities. This would be expected since these photons are absorbed near the back of the device and must travel the entire length of device without recombining to be collected. As the bias increases, this distance also increases since the electric field due to the built-in potential at the front of the device spans a smaller distance. The greater distance the electrons must travel without the assistance of an electric field increases recombination and hence the QE ratio decreases.

When the Schottky barrier height increases (Figure 33), however, the variation in QE ratio for different doping densities becomes evident. The ratio decreases as the doping density decreases. Also, the ratio decreases more for long wavelengths than for short wavelengths since the long-wavelength photons are absorbed in the lightly doped region and carrier collection is affected more by variations in doping and barrier height in this region.

4.2.2 – Effects of Grading at the Back Interface

The next set of simulations examine the effects of band gap grading near the back contact to improve device performance when degraded by a Schottky barrier contact and low doping. A barrier height of 0.3 eV was used and the back-region doping density was varied from 10^{12} cm^{-3} to 10^{15} cm^{-3}. The band gap was changed a total of 0.4 eV over distances of 100 nm, 300 nm, and 500 nm. The IV characteristics are summarized in Figure 34.

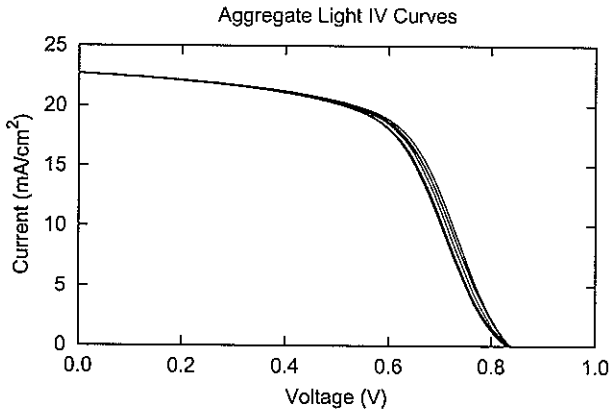

Figure 34: Aggregate IV curves due to doping and grading variations

From the IV characteristics, it appears that little improvement in the short-circuit current or open-circuit voltage were obtained through the use of band gap grading. However, the fill factor does improve, as indicated by the broadening of the curve family in Figure 34. To better analyze these changes, the quantum efficiency ratio is plotted for various back-region doping densities and grading amounts. Figure 35 shows the changes due to grading when the back region is doped the same as the bulk of the absorber (10^{15} cm^{-3}). Little change can be observed due to the grading. When the back region doping density is decreased to 10^{13} cm^{-3}, some improvement at the long wavelengths can be observed, as shown in Figure 36. However, when the back region doping density is decreased further, to 10^{12} cm^{-3}, the improvements due to grading are very evident (Figure 37).

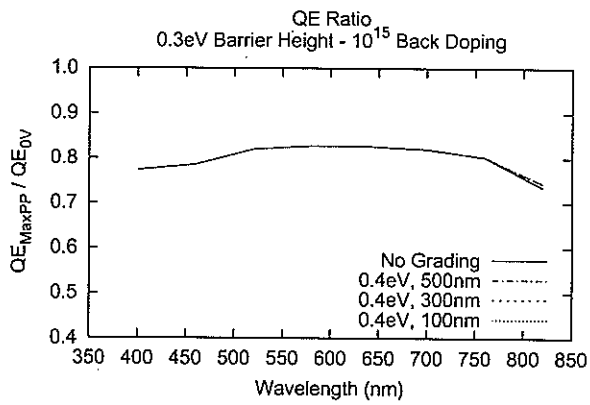

Figure 35: QE ratio for band gap grading, 10^{15} back doping

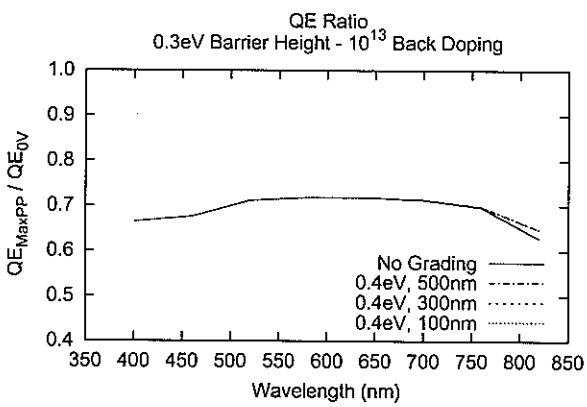

Figure 36: QE ratio for band gap grading, 10^{13} back doping

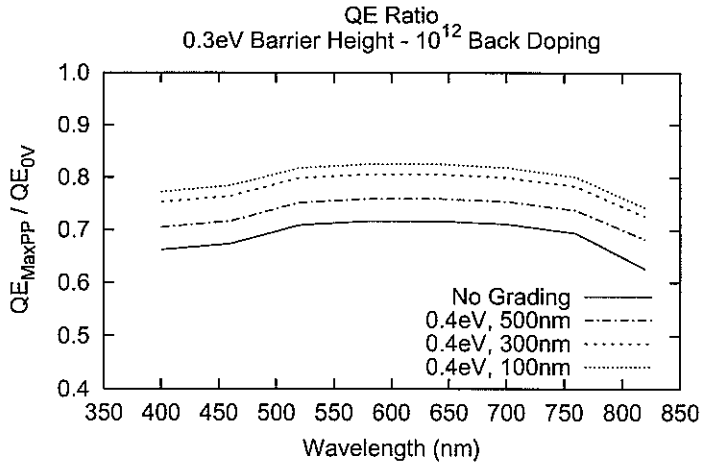

Figure 37: QE ratio for band gap grading, 10^{12} back doping

These results show that band gap grading at the back interface does improve the photovoltaic performance of the device when operated at the maximum power point. However, the grading is only effective when the doping density is low, which might result from imperfect contact formation at the back. Also, the improvements are greatest when the grading distance is the smallest and, therefore, the electric field is the strongest. These simulations also show that the performance of a device with a lightly doped back region can be made comparable to the performance of a device with a more highly doped back region with the use of band gap grading, as shown in Figure 38. The grading at the back interface helps to collect current which would otherwise be lost to the band bending at the back.

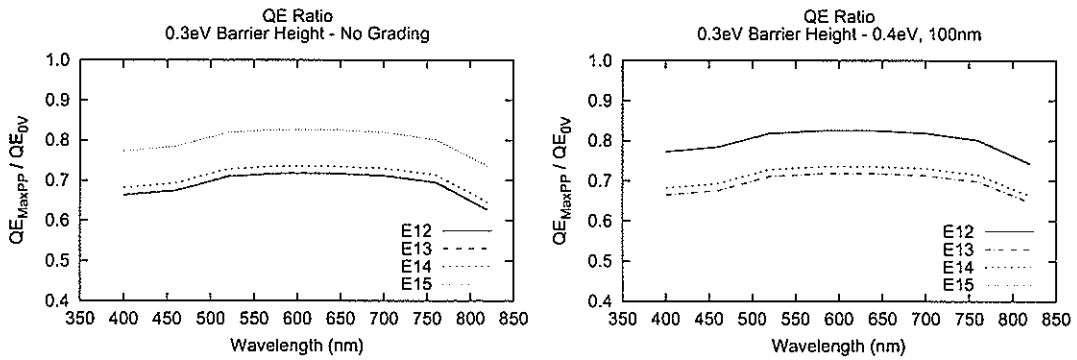

Figure 38: Improvements in QE ratio versus back-region doping

4.2.3 – Comparisons to Experimental Data

To validate the previous simulation results, experimental measurements were examined. These measurements were taken by Dr. Vikram Dalal using CdTe device samples provided by the University of Delaware. Figure 39 shows the IV curve for sample 1.2(A1) before any heat treatments. Figure 40 and Figure 41 show IV curves for the same sample after 90 minutes and 165 minutes, respectively, at 110°C. The characteristic bending of the IV curve near the open-circuit voltage is evident from these curves as the heating time increases.

Based on the previous simulation data, this data can be interpreted as indicating the presence of a Schottky barrier at the back contact, producing the double diode characteristic. A lightly doped region might also be present, enhancing the effects. The QE ratio data, shown in Figure 42, provides some insight into this. Since the QE ratio difference is greatest at the long wavelengths, as in the simulation data in Figure 33, a lightly doped region is likely present near the back contact.

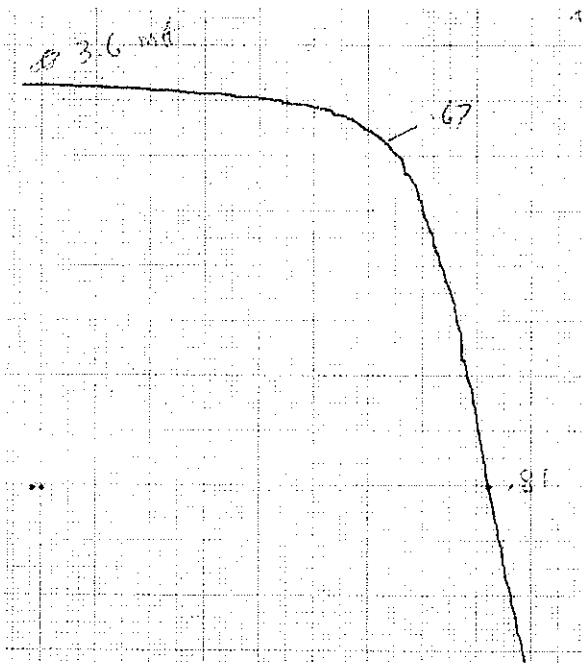

Figure 39: IV curve for sample 1.2(A1) Initial (V. Dalal)

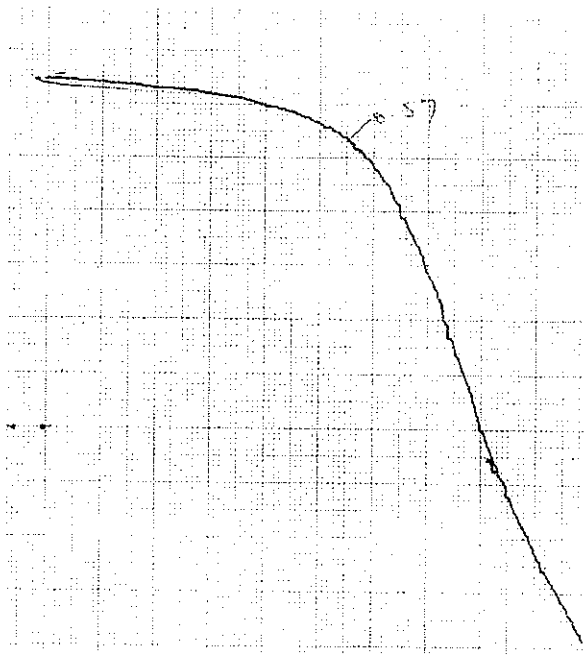

Figure 40: IV curve for sample 1.2(A1)
90 minutes @ 110°C (V. Dalal)

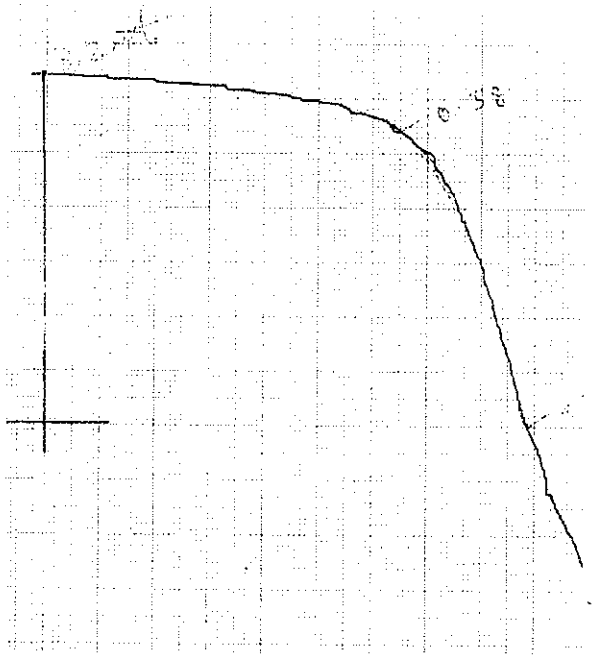

Figure 41: IV curve for sample 1.2(A1)
165 minutes @ 110°C (V. Dalal)

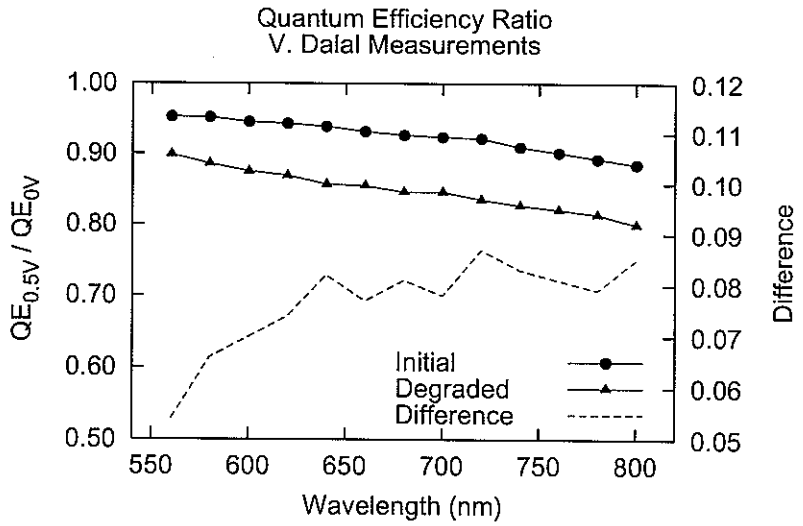

Figure 42: QE ratio data for sample 1.2(A2) (V. Dalal)

The significance of these simulation results lies in understanding and improving the stability of CdTe solar cells. The performance of CdTe solar cells has been known to degrade under conditions of light illumination and module heating, conditions that may occur when the modules are used in a hot desert environment [12]. Typically, the fill factor is reduced significantly and a kink in the IV curve arises near the open-circuit voltage (Appendix B).

Until now, the cause of this kink was unclear. However, the simulation data shows conclusively that the effect is due to a combination of a back Schottky barrier and a doping reduction. This reduction in doping may be explained by diffusion of some impurity from the back contact into the p-type absorber material upon heating to relatively low temperatures in the presence of light.

This work has also shown that the effects of this counterdoping due to contact-induced impurity diffusion may be alleviated by using a graded band gap interface at the back contact. One possible design would be to use a graded band gap at the back contact followed by a highly p-doped ZnTe back contact layer. The unwanted changes in fill factor upon light and heat induced degradation can be almost totally eliminated.

5 – CONCLUSION

Through the use of numerical simulations with the AMPS-1D simulator, the performance of various CdTe based photovoltaic devices has been studied. The effectiveness of these simulations arises in the ability to control individual material parameters precisely and without necessarily changing other parameters. While this may lead to unrealistic parameter sets, it does help provide insight into the effects of changing that one parameter. For this reason, relative changes are more meaningful than the exact numbers unless extensive calibration of the simulations is performed. Even then, there may still be some uncertainty due to the modeling and simulation process.

In this research, both the front and back interfaces to the CdTe absorber layer were studied. For the front interface, grading of the band gap was examined, both in terms of unintentional interdiffusion between the materials and intentional introduction of grading by varying the material composition. In both cases, the open-circuit voltage dropped as the band gap was graded over a longer distance. However, the fill factor changed differently based on the presence of the conduction band offset. When the offset was present, the fill factor degraded for moderate grading distances due to kinking in the IV curve. This kinking resulted from the grading induced effective field in the conduction band. At large grading distances, this kinking was less important and hence the fill factor improved. For the case without any band offset in the conduction band, representing interdiffusion at the interface, the fill factor improves for moderate grading distances. However, as the grading distance increases, the fill factor begins to drop due to reductions in both the short-circuit current and the open-circuit voltage. The spectral response was also shown to degrade with increased grading, matching experimental observations of devices with excessive interdiffusion between the CdS and CdTe layers.

For the back interface, a Schottky barrier contact was used. This caused a degradation in the IV characteristics, most notably the flattening of the IV curve near the open-circuit voltage. These effects became more noticeable as the barrier height was increased. A lightly doped region near the back contact was also shown to degrade the QE ratio, especially at long wavelengths. Band gap grading was again investigated as a possible

improvement mechanism. The grading was shown to improve the performance of the device by enhancing the QE ratio and, therefore, the carrier collection efficiency.

These simulation results were then correlated with experimental data, showing the characteristic IV curve and QE ratio degradation after heating the sample. The simulations help explain the experimental observations by revealing the presence of a Schottky barrier and a lightly doped region at the back contact after light and heat induced degradation. This is the first time that a systematic study of the parameter space using AMPS has been able to explain the observed experimental phenomena related to the degradation of the back contact in CdTe photovoltaic devices. The simulations also show how to improve the back contact using a combination of a graded band gap at the back of the device and a heavily doped p-type ZnTe back contact.

APPENDIX A. SAMPLE AMPS CASE

Sample AMPS case for CdS, (Zn,Cd)Te, ZnTe device.

PARAMETERS THAT APPLY TO THE ENTIRE DEVICE

MODEL	DOS	MINGRID	0.5
PHIBO	0.07	PHIBL	2.22
SNO	1.00e+007	SNL	1.00e+007
SPO	1.00e+007	SPL	1.00e+007
RF	0.00	RB	0.00
T	300.0	DEVWIDTH	3.2000

VOLTAGE BIASING

START	-1.50	END	0.50	STEP1	0.05
STEP2	0.05	STEP3	0.20	STEP4	0.50
SWITCH1	0.01	SWITCH2	3.00	SWITCH3	5.00

ILLUMINATION PARAMETERS

LIGHT	YES	ANALYSIS	LIGHT ONLY
LIGHT-X	1.00000	NWAVES	27
LAMBDA(1)	0.900	FLUX	7.310e+015
LAMBDA(2)	0.880	FLUX	7.970e+015
LAMBDA(3)	0.860	FLUX	8.340e+015
LAMBDA(4)	0.840	FLUX	8.020e+015
LAMBDA(5)	0.820	FLUX	7.200e+015
LAMBDA(6)	0.800	FLUX	8.350e+015
LAMBDA(7)	0.780	FLUX	8.600e+015
LAMBDA(8)	0.760	FLUX	8.200e+015
LAMBDA(9)	0.740	FLUX	8.690e+015
LAMBDA(10)	0.720	FLUX	8.050e+015
LAMBDA(11)	0.700	FLUX	8.650e+015
LAMBDA(12)	0.680	FLUX	8.640e+015
LAMBDA(13)	0.660	FLUX	9.360e+015
LAMBDA(14)	0.640	FLUX	9.200e+015
LAMBDA(15)	0.620	FLUX	9.130e+015
LAMBDA(16)	0.600	FLUX	8.710e+015
LAMBDA(17)	0.580	FLUX	8.470e+015
LAMBDA(18)	0.560	FLUX	8.640e+015
LAMBDA(19)	0.540	FLUX	8.490e+015
LAMBDA(20)	0.520	FLUX	8.040e+015
LAMBDA(21)	0.500	FLUX	7.850e+015
LAMBDA(22)	0.480	FLUX	7.710e+015
LAMBDA(23)	0.460	FLUX	7.320e+015
LAMBDA(24)	0.440	FLUX	5.780e+015
LAMBDA(25)	0.420	FLUX	4.860e+015
LAMBDA(26)	0.400	FLUX	3.940e+015
LAMBDA(27)	0.380	FLUX	2.690e+015

PARAMETERS FOR LAYER 1 - n - CdS

General Parameters					
WIDTH	100.0	MAXGRID	8.0	GRIDPTS	36
EPS	9.00	NA	0.00e+000	NC	1.80e+019
MUN	350.0000	ND	n/a	NV	2.40e+018
MUP	50.0000	EG	2.42	CHI	4.50
DLVS	1	ALVS	0	EGOPT	2.40000
DLVSG	1	ALVSG	0		
Band Tails					
SHAPE	V-SHAPED	GDO	1.00e+003	GAO	1.00e+003
ED	0.01	EA	0.01	TSIG/ND	1.00e-015
TSIG/PD	1.00e-017	TSIG/NA	1.00e-017	TSIG/PA	1.00e-015
Discrete Defects					
ND	1.00e+018	EDON	0.05	WDSD	0.00
DSIG/ND	1.00e-030	DSIG/PD	1.00e-030		
Gaussian Defects					
NDG	1.00e+013	EDONG	1.24	WDSDG	0.01
GSIG/ND	5.00e-010	GSIG/PD	5.00e-011		

PARAMETERS FOR LAYER 2 - p - (Cd,Zn)Te

General Parameters					
WIDTH	3000.0	MAXGRID	50.0	GRIDPTS	278
EPS	9.40	NA	n/a	NC	7.50e+017
MUN	500.0000	ND	0.00e+000	NV	1.80e+018
MUP	60.0000	EG	1.50	CHI	4.28
DLVS	0	ALVS	1	EGOPT	1.50000
DLVSG	0	ALVSG	1		
Band Tails					
SHAPE	V-SHAPED	GDO	1.00e+003	GAO	1.00e+003
ED	0.01	EA	0.01	TSIG/ND	1.00e-015
TSIG/PD	1.00e-017	TSIG/NA	1.00e-017	TSIG/PA	1.00e-015
Discrete Defects					
NA	1.00e+015	EACP	0.05	WDSA	0.00
DSIG/NA	1.00e-030	DSIG/PA	1.00e-030		
Gaussian Defects					
NAG	1.00e+013	EACPG	0.76	WDSAG	0.01
GSIG/NA	6.25e-011	GSIG/PA	6.25e-010		

PARAMETERS FOR LAYER 3 - p+ - ZnTe

General Parameters					
WIDTH	100.0	MAXGRID	8.0	GRIDPTS	36
EPS	9.00	NA	n/a	NC	7.50e+017
MUN	1.0000	ND	0.00e+000	NV	1.80e+018
MUP	1.0000	EG	2.25	CHI	3.50
DLVS	0	ALVS	1	EGOPT	2.25000
DLVSG	0	ALVSG	0		
Band Tails					
SHAPE	V-SHAPED	GDO	1.00e+003	GAO	1.00e+003
ED	0.01	EA	0.01	TSIG/ND	1.00e-015
TSIG/PD	1.00e-017	TSIG/NA	1.00e-017	TSIG/PA	1.00e-015
Discrete Defects					
NA	1.00e+018	EACP	0.05	WDSA	0.00
DSIG/NA	1.00e-030	DSIG/PA	1.00e-030		

ABSORPTION COEFFICIENTS

LAMBDA	LAYER 1 ALPHA	LAYER 2 ALPHA	LAYER 3 ALPHA
0.900	2.500e+002	1.000e+001	1.000e+001
0.880	2.500e+002	3.000e+001	3.000e+001
0.860	2.500e+002	2.000e+002	2.000e+002
0.840	2.500e+002	1.000e+003	1.000e+003
0.820	2.500e+002	1.340e+004	1.340e+004
0.800	2.600e+002	1.980e+004	1.980e+004
0.780	2.700e+002	2.480e+004	2.480e+004
0.760	3.000e+002	2.920e+004	2.920e+004
0.740	3.400e+002	3.320e+004	3.320e+004
0.720	4.000e+002	3.690e+004	3.690e+004
0.700	5.000e+002	4.050e+004	4.050e+004
0.680	6.000e+002	4.400e+004	4.400e+004
0.660	8.000e+002	4.740e+004	4.740e+004
0.640	1.000e+003	5.080e+004	5.080e+004
0.620	1.900e+003	5.430e+004	5.430e+004
0.600	4.000e+003	5.830e+004	5.830e+004
0.580	7.000e+003	6.300e+004	6.300e+004
0.560	1.500e+004	6.860e+004	6.860e+004
0.540	8.000e+004	7.550e+004	7.550e+004
0.520	1.500e+005	8.420e+004	8.420e+004
0.500	1.800e+005	9.520e+004	9.520e+004
0.480	1.800e+005	1.090e+005	1.090e+005
0.460	1.820e+005	1.270e+005	1.270e+005
0.440	1.850e+005	1.510e+005	1.510e+005
0.420	1.870e+005	1.810e+005	1.810e+005
0.400	1.880e+005	2.210e+005	2.210e+005
0.380	1.900e+005	2.420e+005	2.420e+005

APPENDIX B. DEGRADED IV CURVES

The following dark and light IV curves show the degradations due to light and heat stress performed at various biases, as reported by P.V. Meyers and J.E. Phillips at the University of Delaware [12].

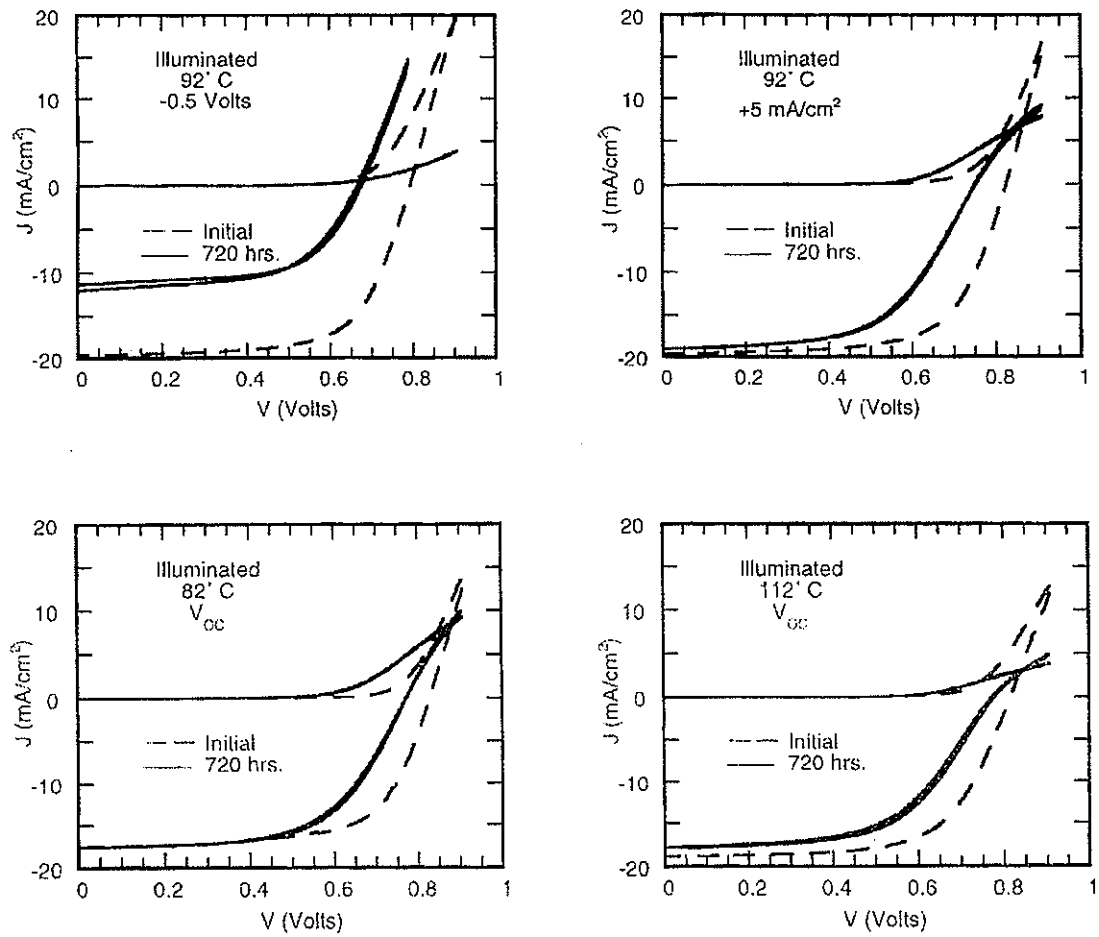

REFERENCES

[1] A Fahrenbruch, R. Bube, "Fundamentals of Solar Cells", Academic Press, 1983.

[2] D. Lillington, H. Cotal, J. Ermer, D. Friedman, T. Moriarty, A. Duda, "32.3% efficient triple junction $GaInP_2$/GaAs/Ge concentrator solar cells", *35th Energy Conversion Engineering Conference and Exhibit*, pp. 516-521, 2000.

[3] H. Ohyama, "16.0% Efficient Thin-Film CdS/CdTe Solar Cells", *Proc. 26th IEEE Photovoltaic Specialists Conference*, pp. 343-346, 1997.

[4] B. Basol, "Thin Film CdTe Solar Cells – A Review", *Proc. 21st IEEE Photovoltaic Specialists Conference*, pp. 588-594, 1990.

[5] T. Nishio, "Thin-film CdS/CdTe Solar Cell with 15.05% Efficiency", *Proc. 25th IEEE Photovoltaic Specialists Conference*, pp. 953-956, 1996.

[6] C. Hu, R. White, *Solar Cells*, McGraw-Hill, 1983.

[7] S. Fonash, S. Ashok, "An additional source of photovoltage in photoconductive materials", *Applied Physics Letters*, vol. 35, no. 1, pp. 535-537, 1979.

[8] R. Bohn, "RF Sputtered Films of Cu-doped And N-doped ZnTe", *Proc. 24th IEEE Photovoltaic Specialists Conference*, pp. 354-356, 1994.

[9] T. Chu, S. Chu, "Thin-film II-VI photovoltaics", *Solid-State Electronics*, vol. 38, no. 3, pp. 533-549, 1995.

[10] R. Dhere, "Influence of CdS/CdTe interface properties on the device properties", *Proc. 26th IEEE Photovoltaic Specialists Conference*, pp. 435-438, 1997.

[11] A. Fischer, "Properties of CdS_xTe_{1-x} alloy films", *Proc. 26th IEEE Photovoltaic Specialists Conference*, pp. 447-450, 1997.

[12] P. Meyers, J. Phillips, "Stress Testing of CdTe Solar Cells", *Proc. 25th IEEE Photovoltaic Specialists Conference*, pp. 789-792, 1996.